

Article

# Improved Catalytic Properties of *Thermomyces lanuginosus* Lipase Immobilized onto Newly Fabricated Polydopamine-Functionalized Magnetic Fe<sub>3</sub>O<sub>4</sub> Nanoparticles

Yanhong Bi <sup>1,2</sup>, Zhaoyu Wang <sup>2</sup>, Rui Zhang <sup>2</sup>, Yihan Diao <sup>2</sup>, Yaoqi Tian <sup>1</sup> and Zhengyu Jin <sup>1,\*</sup>

<sup>1</sup> State Key Laboratory of Food Science and Technology, School of Food Science and Technology, Jiangnan University, Wuxi 214122, China; byhfood@126.com (Y.B.); yqtian@jiangnan.edu.cn (Y.T.)

<sup>2</sup> School of Life Science and Food Engineering, Huaiyin Institute of Technology, Huai'an 223003, China; biowzy@126.com (Z.W.); zhangrui.cq@foxmail.com (R.Z.); diaoyihan@outlook.com (Y.D.)

\* Correspondence: fpcenter@jiangnan.edu.cn

Received: 11 April 2020; Accepted: 18 May 2020; Published: 24 May 2020



**Abstract:** In this study, magnetic Fe<sub>3</sub>O<sub>4</sub> nanoparticles coated with polydopamine possessing abundant amino groups (Fe<sub>3</sub>O<sub>4</sub>@PDA) were conveniently prepared, detailed, and characterized, and then firstly used as a supporting matrix for immobilizing *Thermomyces lanuginosus* lipase (Fe<sub>3</sub>O<sub>4</sub>@PDA@TLL). The effects of some crucial factors on the immobilization efficiency were investigated and the optimal protein loading and activity recovery were found to be 156.4 mg/g and 90.9%, respectively. Characterization studies revealed that Fe<sub>3</sub>O<sub>4</sub>@PDA@TLL displayed a broader pH and temperature adaptability as compared to the free TLL, which allows its use at wider ranges of reaction conditions. With regard to the stabilities, the immobilized TLL clearly displayed improved pH, thermal, and solvent tolerance stabilities compared to the free enzyme, suggesting that the biocompatible Fe<sub>3</sub>O<sub>4</sub>@PDA might be an outstanding material for immobilizing TLL and acting as alternative support for different enzymes.

**Keywords:** magnetic nanoparticle; immobilization; *Thermomyces lanuginosus* lipase; stability

## 1. Introduction

Enzyme immobilization has been described as a facile and powerful tool for improving the properties of enzymes. Accordingly, it has been applied extensively in the areas of the food, pharmaceutical, and cosmetic industries [1,2]. Physical adsorption, entrapment/encapsulation, cross-linking, and covalent binding are among the typical immobilization approaches for the coupling of the enzyme with carrier material [1], which is often crucial to optimizing enzyme behavior in industrial processes. Though the immobilized enzymes have been well known for over four decades, they are still largely restricted to industrial-scale applications, particularly for use in nonaqueous enzymatic catalysis systems because of their inadequate reusability, operational stability, recovery, and shelf-life [3,4].

Recent advances in modern nanoscience allow for a variety of choices in exploring novel immobilization strategies to overcome the aforementioned drawbacks of the enzymes, which may offer new possibilities for establishing sustainable, highly efficient, and overall cost-effective industrial processes [5–7]. Among the available nano-immobilization protocols, surface-modified magnetic nanoparticles (MNPs) possessing excellent characteristics of biocompatibility, chemical stability, and dispersity are receiving considerable attention as robust immobilization supports [3]. Modified materials—including polydopamine (PDA), chitosan, and cellulose—have proved to be

eminent modified agents for masking the magnetic nanoparticles because of their outstanding advantages derived from the existence of numerous functional groups such as amino, hydroxyl, and hydroxymethyl groups, which can be coupled easily with the enzyme protein [8–10]. For example, Wang et al. investigated pullulanase immobilization using  $\text{Fe}_3\text{O}_4$  MNPs modified with functional groups and found that ionic adsorption of pullulanase on  $\text{Fe}_3\text{O}_4$ @PDA-polyethyleneimine-glycidyltrimethylammonium gave a high performance and a durable catalyst [11]. Based on the surface available functional or functionalized entities, Lou et al. explored a series of convenient and efficient nanoparticle-based catalytic supports like  $\text{Fe}_3\text{O}_4$ @polydopamine,  $\text{Fe}_3\text{O}_4$ @cellulose, and  $\text{Fe}_3\text{O}_4$ @chitosan@cellulose to immobilize lipase and papain by physical adsorption or covalent coupling method [3,5]. Their further characterization indicated that the catalytic features such as activity, organic solvent tolerance, and reusability were substantially improved in their respective catalytic systems.

*Thermomyces lanuginosus* lipase (TLL) is a versatile biocatalyst and is widely used in the oleochemical industry, biodiesel production, organic synthesis, and environmental protection [12]. However, like most of the industrial enzymes, TLL also suffers from leaching from the carrier support, easy denaturation by organic solvent, and poor recyclability, inevitably resulting in loss of their catalytic activities and extremely high cost [13]. With the development of the nanoparticle-based immobilization strategy, magnetic nano- $\text{Fe}_3\text{O}_4$  has emerged as a desirable alternative to traditional materials for assembling immobilized TLL with markedly improved performances [14–16]. Therefore, in this study, we report the development of a novel nanobiocatalyst by using a PDA biomimetic coating to combine TLL with magnetic  $\text{Fe}_3\text{O}_4$  nanoparticle ( $\text{Fe}_3\text{O}_4$ @PDA@TLL). The structural features, catalytic activity, and stability of the free and immobilized enzymes were investigated in detail to characterize their desirable properties. The findings might offer primary guidelines for the enzyme nano-immobilization techniques and are of interest in industrial biotechnology.

## 2. Materials and Methods

### 2.1. Catalysts and Chemicals

*T. lanuginosus* lipase (TLL) was purchased from Novozymes Co., Ltd., China. Dopamine hydrochloride, 2-methyltetrahydrofuran (MeTHF), *p*-nitrophenyl palmitate (*p*-NPP), and *p*-nitrophenol were procured from Aladdin Reagent Co. Ltd. (Shanghai). Choline chloride/glycerol (ChCl/GL, 1:2), choline chloride/ethylene glycol (ChCl/EG, 1:2), choline chloride/urea (ChCl/UR, 1:3), and choline chloride/acetic acid (ChCl/AA, 1:2) were kindly donated by Professor Zhangqun Duan (Academy of State Administration of Grain, China). All other chemicals were of the highest reagent grade commercially available and used as received.

### 2.2. Preparation of $\text{Fe}_3\text{O}_4$ @PDA

The magnetic  $\text{Fe}_3\text{O}_4$  nanoparticles were prepared by a chemical coprecipitation method, as reported earlier, with slight modifications [8]. According to this method, 0.87 g  $\text{FeCl}_3 \cdot 6\text{H}_2\text{O}$  and 0.31 g  $\text{FeCl}_2 \cdot 4\text{H}_2\text{O}$  were dissolved in 25 mL deionized water under the nitrogen atmosphere. The mixture was then placed in a 75 °C water bath with vigorous stirring. Afterwards, 1.5 mol/L NaOH solution was added dropwise and the pH of the solution was maintained at 9.0–10 under continuous stirring for 1.0 h. The precipitated particles were washed with deionized water and dried in a vacuum for 24 h. To prepare PDA-coated  $\text{Fe}_3\text{O}_4$  ( $\text{Fe}_3\text{O}_4$ @PDA), dopamine hydrochloride and  $\text{Fe}_3\text{O}_4$  nanoparticles, which were dispersed in deionized water for 10 min under sonication, with the molar ratio of 1:1, were mixed and stirred vigorously. The pH of the mixture was adjusted to 8.5 by adding the above NaOH solution. After stirring for 24 h at room temperature, the  $\text{Fe}_3\text{O}_4$ @PDA was formed, collected with an external magnet and rinsed with deionized water repeatedly.

### 2.3. Preparation of Immobilized Lipase

In a typical experiment, 0.4 g of  $\text{Fe}_3\text{O}_4\text{@PDA}$  was added to 12 mL of phosphate buffer (50 mM, pH 8.0) at 25 °C, and 2.4 mL of TLL solution (260 mg/mL) was then added to the sample. The mixture was stirred at 250 rpm for 4.0 h. After the stipulated time, the immobilized sample was recovered and continuously washed until no protein was detected. The enzyme-loaded  $\text{Fe}_3\text{O}_4\text{@PDA}$  was designated as  $\text{Fe}_3\text{O}_4\text{@PDA-TLL}$ . The concentration of the residual TLL in the supernatant and washings was subsequently determined using Bradford's method [17]. The immobilization yield of TLL was calculated using the following equation:

$$Y = [(m_0 - m_1 - m_2)/m_0] \times 100 \quad (1)$$

where  $m_0$  is the mass of TLL protein initially added to the phosphate buffer,  $m_1$  and  $m_2$  are the protein content of the supernatant and wash solution after immobilization. All data in this formula are averages of duplicate experiments.

### 2.4. Assay of Enzyme Activity

The activity of free and immobilized TLL was assayed according to the *p*-nitrophenyl palmitate (*p*-NPP) method with slight modifications [18]. The activity assay was conducted in 1.0 mL Tris-HCl buffer (50 mM, pH 8.0) containing 0.1 mL *p*-NPP solution (a quantity of 30 mg *p*-NPP was dissolved in 10 mL isopropanol). The reaction was initiated with the addition of either 0.1 g immobilized enzyme or 0.1 mL TLL solution and incubated at 37 °C and 250 rpm for 10 min. After a predetermined time, the reaction was stopped by adding 5.0 mL of 95% ethanol. The absorbance of the reaction mixture was determined at 410 nm and the activity was calculated. One unit of activity (U) was defined as the amount of enzyme required to produce 1.0  $\mu\text{mol}$  *p*-nitrophenol (*p*-NP) in 1.0 min under the above conditions. The specific activities of the free TLL and  $\text{Fe}_3\text{O}_4\text{@PDA-TLL}$  were 3921 U/mL and 8022 U/g, respectively.

### 2.5. Surface Characterization of the Immobilized Lipase

The morphologies of various pristine and lipase-couple nanoparticles were envisaged using a transmission electron microscopy (TEM, Tecnai G2 20) with an accelerating voltage of 200 kV. The Fourier Transform infrared spectroscopy (FT-IR spectra) was obtained with a Nicolet 670 spectrometer using KBr pellets. A PANalytical X'Pert Pro instrument using Cu KR (k) 0.154 nm radiation carried out small-angle X-ray diffraction (XRD) measurements. The surface composition was performed on X-ray photoelectron spectroscopy (XPS) with an ESCALAB-250 electron spectrometer with 13 kV high pressure and 20 mA electric current using Mg  $K\alpha$  as radiation.

### 2.6. Effect of pH and Temperature on the Free and Immobilized Lipase

The optimum reaction pH and temperature of the free and immobilized lipases were determined as the relative activity in Tris-HCl buffer with a variety of pH (from 6.5 to 9.0) and temperature (from 10 °C to 55 °C), following the same procedure as in Section 2.4. The highest activity of the lipase incubated under different conditions was defined as 100%. All the experiments were repeated three times and the standard deviation was calculated.

### 2.7. pH Stability Studies of Free and Immobilized Lipase

The pH stabilities of free and immobilized lipase were carried out by incubating them in Tris-HCl buffer (50 mM) adjusted to various pH values (pH = 6.0–10) at 25 °C for 12 h. Then the residual activity was determined, as described in Section 2.4, and the activity of the lipase without incubation was defined as 100% (the method for measuring and defining residual enzyme activity was the same with thermal and solvent tolerance stability studies).

### 2.8. Thermal Stability Studies of Free and Immobilized Lipase

The thermal stabilities were examined by incubating the free or immobilized TLL in Tris-HCl buffer (50 mM, pH = 8.0) at different temperatures (25–80 °C) for 12 h.

### 2.9. Solvent Tolerance Stability Studies of Free and Immobilized Lipase

Solvent tolerance stabilities were measured after the lipases were incubated in seven typical organic solvents, such as acetonitrile, ethanol, ChCl/GL (1:2), ChCl/EG (1:2), ChCl/UR (1:3), and ChCl/AA (1:2) for 12 h at 25 °C.

### 2.10. Operational Stability Studies of Free and Immobilized Lipase

The operational stabilities of immobilized TLL during the batch hydrolysis of *p*-NPP were investigated. When the maximum *p*-NP yield was achieved, the Fe<sub>3</sub>O<sub>4</sub>@PDA-TLL was separated by filtration and washed three times. Then, the reused enzyme was added into the fresh reaction mixture at 25 °C, followed by the assay of its activity and maximum product yield. The initial activity obtained in the first batch was defined as 100 %.

## 3. Results and Discussion

### 3.1. Preparation and Characterization of Fe<sub>3</sub>O<sub>4</sub>@PDA@TLL

Several characterization techniques were used to identify the topological/chemical structures and other physicochemical properties of the bare and lipase-coupled nanoparticles. The morphology and size of bare Fe<sub>3</sub>O<sub>4</sub>, Fe<sub>3</sub>O<sub>4</sub>@PDA, and Fe<sub>3</sub>O<sub>4</sub>@PDA@TLL were first analyzed by TEM. The TEM images are portrayed in Figure 1. The Fe<sub>3</sub>O<sub>4</sub> nanoparticles were mostly regular spherical or ellipsoidal shape with an average diameter of 18.7 nm measured using a dynamic laser scattering particle size (DLS) analyzer (Brookhaven, NanoBrook 90Plus, USA), as shown in Figures 1A and 2A. After surface modification with a polymeric shell by self-assembly of PDA in alkaline aqueous solution, it was seen that the magnetic microspheres were wrapped with a thin PDA layer and showed a tendency to aggregate due to the interaction between PDA and magnetic nanoparticles), conforming to the formation of the uniform PDA shell, see Figure 1B. Further, the introduction of enzyme protein to PDA-coated Fe<sub>3</sub>O<sub>4</sub> nanoparticles through the Schiff base reaction between amine groups shows no distinct changes in the morphology of the Fe<sub>3</sub>O<sub>4</sub>@PDA and Fe<sub>3</sub>O<sub>4</sub>@PDA@TLL, as seen in Figure 1C, but a relatively aggregative appearance was observed compared to the precursor Fe<sub>3</sub>O<sub>4</sub> particles. This is in good agreement with the previous results [19,20]. Moreover, based on the analysis of the size distribution, the mean diameters of aggregated Fe<sub>3</sub>O<sub>4</sub>@PDA and Fe<sub>3</sub>O<sub>4</sub>@PDA@TLL were estimated to be 24.4 and 29.8 nm, as shown in Figure 2B and 2C, respectively, which were obviously larger than that of the MNPs and consistent with those recorded in the TEM images.

XPS was applied to analyze the chemical compositions of all types of the bare and enzyme-attached nanoparticles as seen in Figure 3A. Wide scan XPS spectra indicated that the characteristic peaks of Fe 2*p* (Fe 2*p*<sub>1/2</sub> 723.97 eV, Fe 2*p*<sub>3/2</sub> 709.97 eV) and O 1s (529.97 eV) were detected in all the examined samples, which were in consonance with the previous reports [21]. The additional binding energy peaks of C 1s of 283.97 eV and N 1s of 400.97 eV appeared in Fe<sub>3</sub>O<sub>4</sub>@PDA and a significant enhancement in Fe<sub>3</sub>O<sub>4</sub>@PDA@TLL nanocomposites corroborated the successful grafting of PDA and enzyme protein onto the nano-Fe<sub>3</sub>O<sub>4</sub> particles [8].

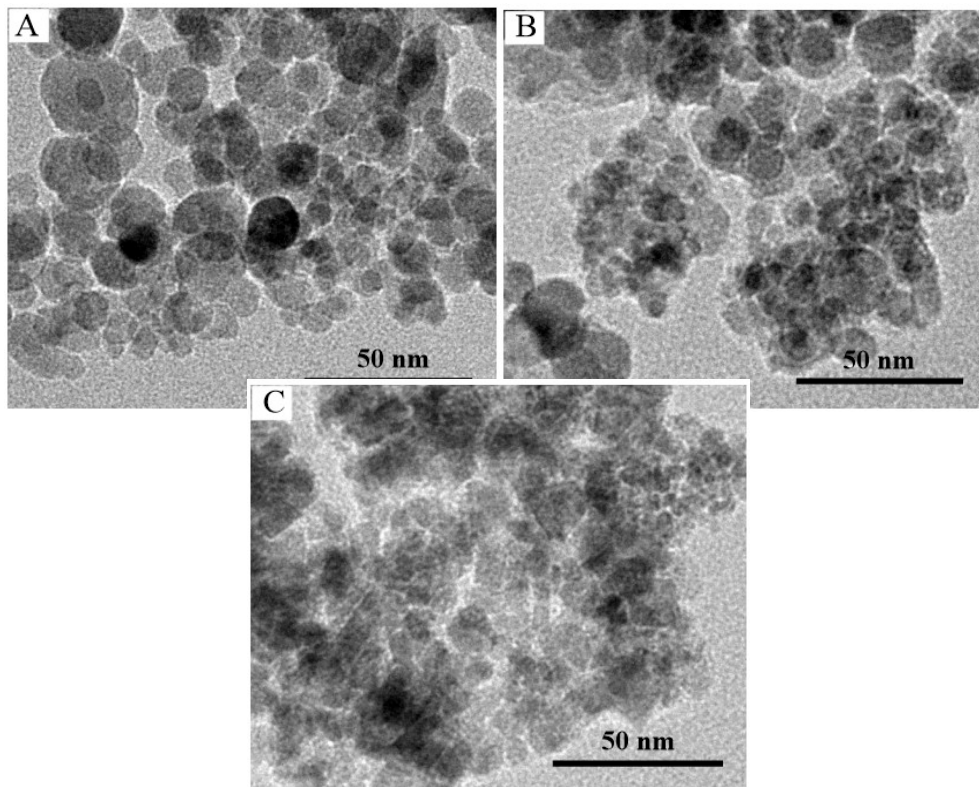


**Figure 1.** TEM images of Fe<sub>3</sub>O<sub>4</sub> (A), Fe<sub>3</sub>O<sub>4</sub> nanoparticles coated with polydopamine possessing abundant amino groups (Fe<sub>3</sub>O<sub>4</sub>@PDA) (B), and the aforementioned used as a supporting matrix for immobilizing *Thermomyces lanuginosus* lipase (Fe<sub>3</sub>O<sub>4</sub>@PDA@TLL) (C).

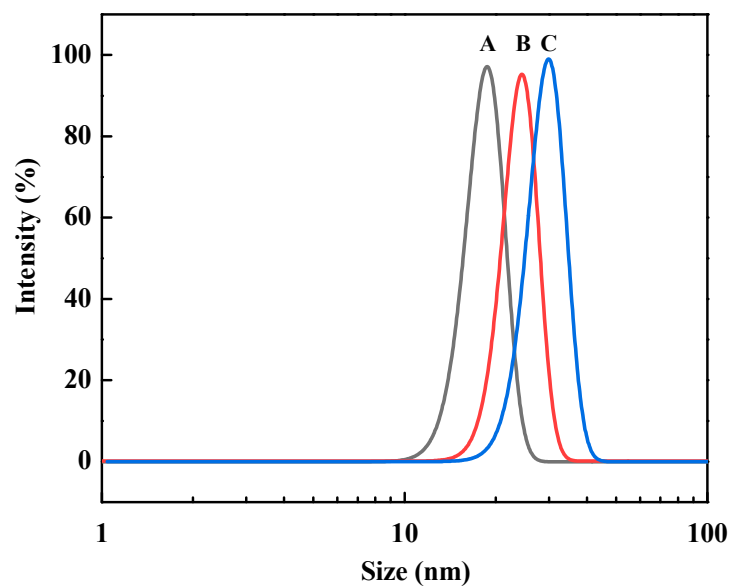


**Figure 2.** Size distribution of Fe<sub>3</sub>O<sub>4</sub> (A), Fe<sub>3</sub>O<sub>4</sub>@PDA (B), and Fe<sub>3</sub>O<sub>4</sub>@PDA@TLL (C).

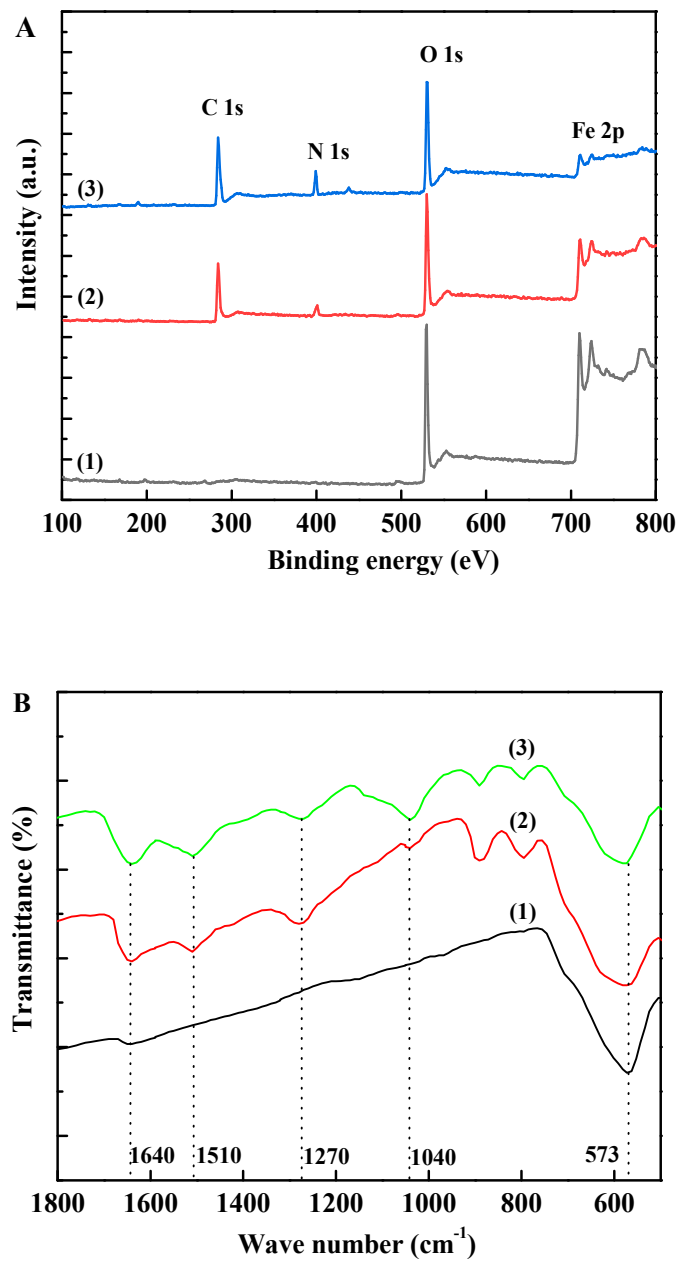
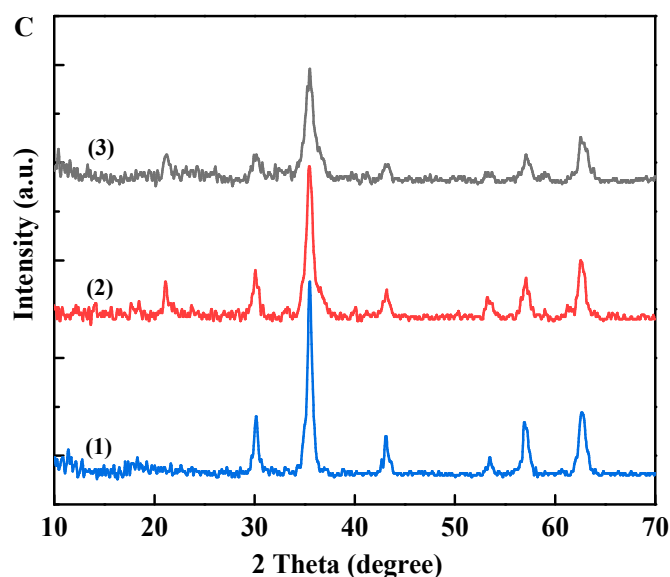


Figure 3. Cont.



**Figure 3.** XPS spectra (A), FT-IR spectra (B), and XRD patterns (C) of  $\text{Fe}_3\text{O}_4$  (1),  $\text{Fe}_3\text{O}_4@PDA$  (2) and  $\text{Fe}_3\text{O}_4@PDA@TLL$  (3).

FT-IR spectra were also obtained to evaluate the immobilized enzyme on the surface of  $\text{Fe}_3\text{O}_4@PDA$ , as seen in Figure 3B. The appearance of a strong absorption band of  $\text{Fe}_3\text{O}_4$  spectra at  $573\text{ cm}^{-1}$  represents the vibration of the Fe-O function group [8]. According to the recent report by Sureshkumar et al. [22], dopamine showed some peak absorptions between  $1000\text{--}1600\text{ cm}^{-1}$ . After the successful functionalization of MNPs with PDA, the stretching vibrations of the carbonyl group at  $1640\text{ cm}^{-1}$ , C=C bending group at  $1510\text{ cm}^{-1}$ , and a phenolic hydroxyl group at  $1270\text{ cm}^{-1}$  in the  $\text{Fe}_3\text{O}_4@PDA$  samples are clearly seen in curves 2 and 3, Figure 3B, proving that PDA shell had been successfully coated on the  $\text{Fe}_3\text{O}_4$  surface [8,21]. Furthermore, the peaks at  $1040\text{ cm}^{-1}$  and  $1510\text{ cm}^{-1}$  assigned to the C-N and C=C bending vibrations, respectively, were broader than those of  $\text{Fe}_3\text{O}_4@PDA$ , which indicated the immobilization of the enzyme onto the support. The results of XRD experiments are shown in Figure 3C. Regarding the  $\text{Fe}_3\text{O}_4$  nanoparticles, the six characteristic peaks at  $2\theta = 30.2^\circ$ ,  $35.5^\circ$ ,  $43.1^\circ$ ,  $53.5^\circ$ ,  $57.0^\circ$ , and  $62.7^\circ$  corresponding to the lattice planes of (220), (311), (400), (422), (511), and (440), respectively, which are typical characteristics of  $\text{Fe}_3\text{O}_4$  [8]. After coating with PDA and immobilization of TLL, the XRD data of  $\text{Fe}_3\text{O}_4@PDA$  and  $\text{Fe}_3\text{O}_4@PDA@TLL$  seen in curves 2 and 3, Figure 3C, reveal that all the main peaks were overlapped with the diffraction peak of the  $\text{Fe}_3\text{O}_4$ , as seen in curve 1, Figure 3C. This fully indicates that the  $\text{Fe}_3\text{O}_4$  cores maintained their crystalline structure in the immobilized complex.

### 3.2. Immobilization of TLL onto $\text{Fe}_3\text{O}_4@PDA$

It is well documented that the immobilization efficiency and activity of the immobilized enzyme are strongly dependent on the immobilization parameters such as the enzyme-support ratio, pH of the solution, or the working temperature. For example, the loading amount of enzyme protein on  $\text{Fe}_3\text{O}_4@PDA$  was increased from  $128.5\text{ mg/g}$  to  $189.3\text{ mg/g}$  as the enzyme-support ratio increased from 0.52 to 2.6, as shown in Figure 4A. The enzyme activity recovery was first increased and then a decreasing tendency was noticed, and the best ratio of enzyme to support proved to be about 1.6 with an activity recovery and a protein loading of 85.5% and  $178.4\text{ mg/g}$ , respectively. Surprisingly, the protein-loading capacity of the  $\text{Fe}_3\text{O}_4@PDA$  is obviously greater than those reported in most literature [14,15,23]. The higher concentration of the initial TLL protein used for immobilization may be responsible for this phenomenon. However, no obvious correlation was observed between the enzyme protein loading and catalytic activity of the immobilized TLL. This is similar to the immobilization of laccase on the magnetic  $\text{Fe}_3\text{O}_4$  nanoparticles [24]. Although the activity recovery of the immobilized enzyme would

be enhanced with the increase in initial enzyme concentration, excessive enzyme protein absorption on the surface of  $\text{Fe}_3\text{O}_4@ \text{PDA}$  forms intensive intermolecular steric hindrance, thus leading to the diffusional restrictions of substrates and products and deactivation of the immobilized enzyme [24].

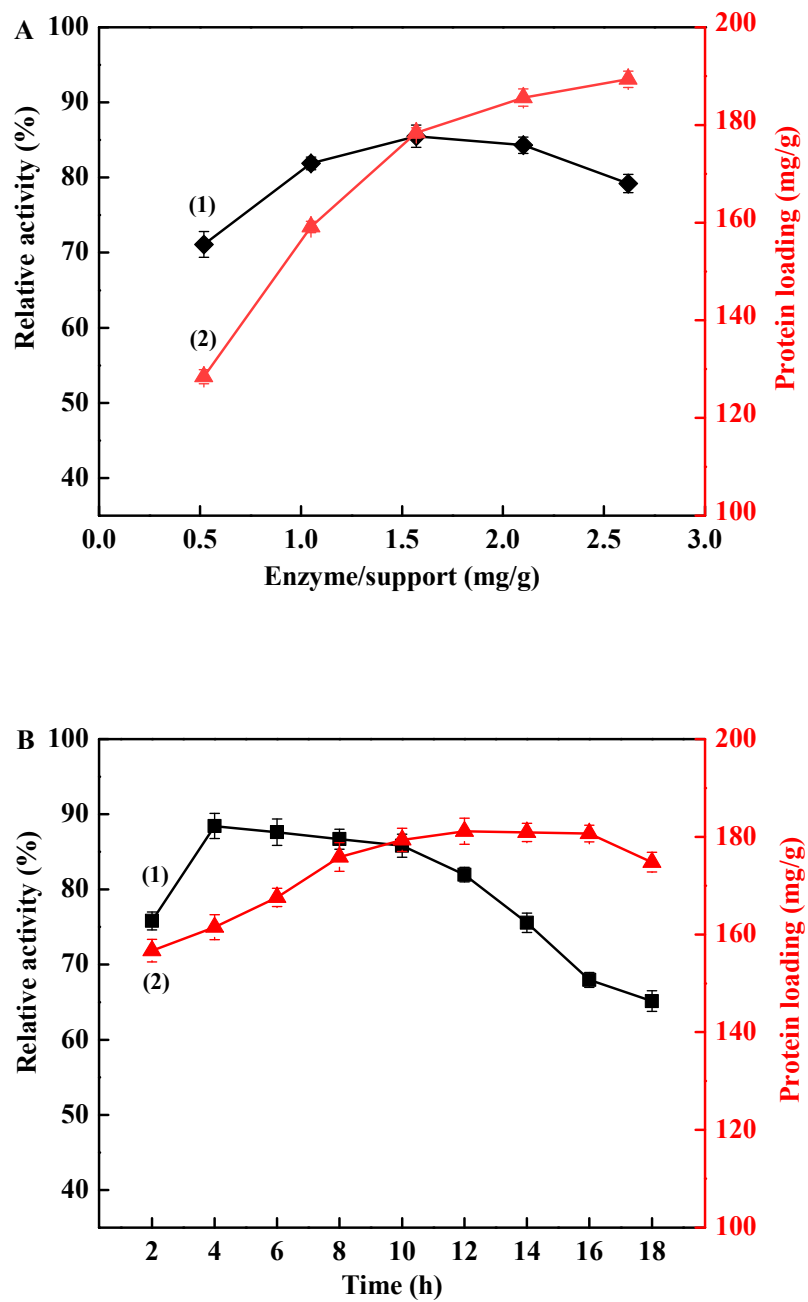
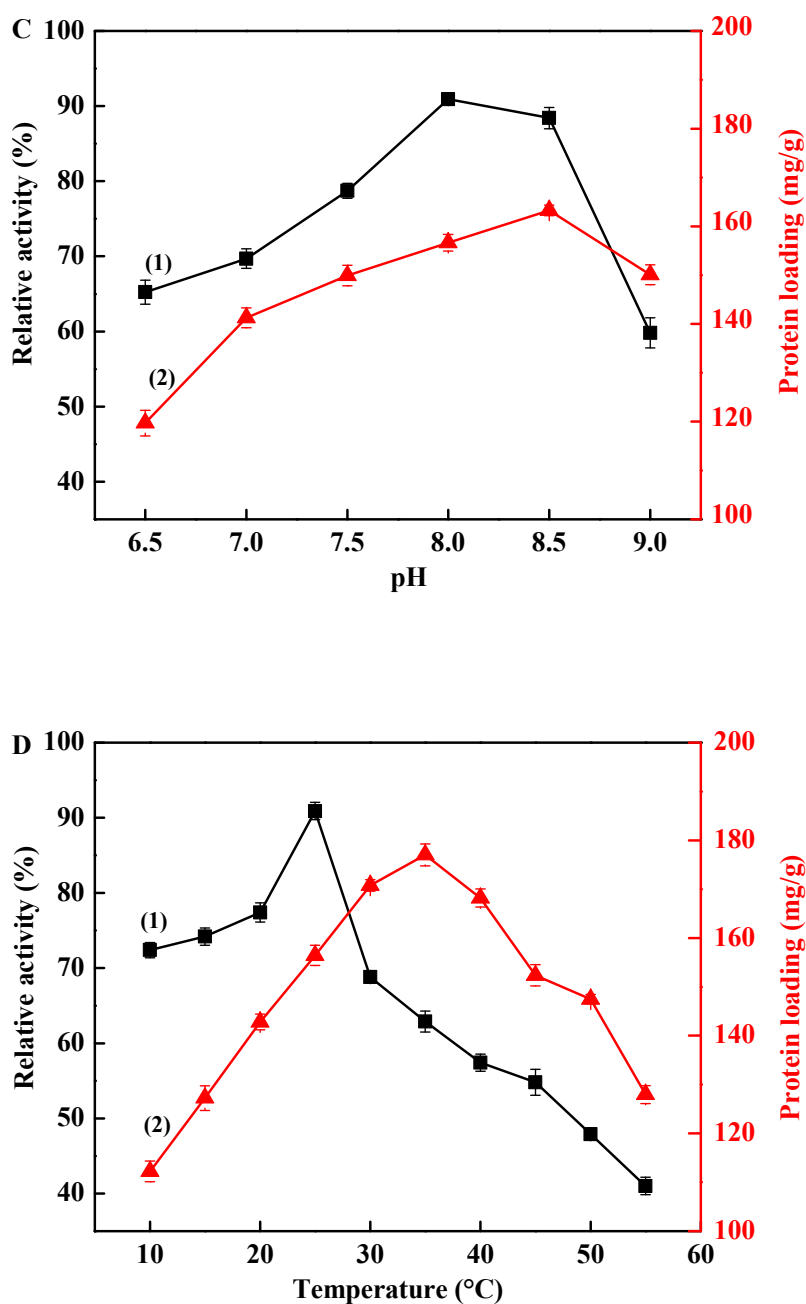


Figure 4. Cont.



**Figure 4.** Effect of immobilization conditions on activity recovery (1) and protein loading (2). (A) Effect of enzyme-support ratio (12 mL phosphate buffer (50 mM, pH 8.5) containing 0.4 g  $\text{Fe}_3\text{O}_4\text{@PDA}$ , different amount of TLL, 25 °C, 10 h); (B) Effect of immobilization time (12 mL phosphate buffer (50 mM, pH 8.5) containing 0.4 g  $\text{Fe}_3\text{O}_4\text{@PDA}$ , 2.4 mL TLL, 25 °C, different immobilization time); (C) Effect of immobilization pH (12 mL phosphate buffer (50 mM, pH 6.5–9.0) containing 0.4 g  $\text{Fe}_3\text{O}_4\text{@PDA}$ , 2.4 mL TLL, 25 °C, 4.0 h); (D) Effect of immobilization temperature (12 mL phosphate buffer (50 mM, pH 8.0) containing 0.4 g  $\text{Fe}_3\text{O}_4\text{@PDA}$ , 2.4 mL TLL, 10–55 °C, 4.0 h).

The effect of coupling time on the immobilization process was also studied and exemplified in Figure 4B. The protein loading on the immobilization material increased with prolonging coupling time up to 12 h, while a reduction in the proportion of residual activity was observed after reaching the plateau coupling reaction time of 4.0 h, with enzyme immobilization and activity retention of 161.5 mg/g and 88.4%, respectively. In consideration of these observations, the optimal coupling time used for TLL lipase conjugation on  $\text{Fe}_3\text{O}_4\text{@PDA}$  was 4.0 h. Of the tested pH values ranging

from 6.5 to 9.0 as depicted in Figure 4C, the alkaline immobilization conditions such as pH 7.5–8.5 seem to be favorable for TLL immobilization on  $\text{Fe}_3\text{O}_4\text{@PDA}$ , retaining about 90.9% of its maximum activity at pH 8.0. Interestingly, the enzyme loadings displayed a gradually increasing trend with the enhancement of pH, indicating that the high pH might be beneficial for protein deposition on the surface of  $\text{Fe}_3\text{O}_4\text{@PDA}$  [21]. Temperature also plays an important role in the immobilization process, influencing not only the activity recovery but also the enzyme loading. As shown in Figure 4D, increasing the temperature from 10 °C to 25 °C brought about a gradual improvement in both the above crucial parameters. The optimum activity recovery and enzyme loading were 90.9% and 156.4 mg/g, respectively. A further increase in temperature resulted in a drastic drop in the activity recovery, presumably due to the partial inactivation of the TLL at high temperatures.

### 3.3. Effect of the pH and Temperature on Free and Immobilized TLL

For a better understanding of the property of the immobilized  $\text{Fe}_3\text{O}_4\text{@PDA@TLL}$ , the effects of pH and temperature were studied on the basis of determining the hydrolysis of *p*-NPP, as shown in Figure 5. For example, the influence of pH ranging from 6.5 to 9.0 was first examined at 25 °C to investigate the optimum pH wherein the enzymes are most active. Results showed that the optimal pH for the free enzyme was 7.5, while after immobilization, the optimal pH for  $\text{Fe}_3\text{O}_4\text{@PDA@TLL}$  shifted to 8.0, as seen in Figure 5A. Unquestionably,  $\text{Fe}_3\text{O}_4\text{@PDA@TLL}$  displayed broader pH adaptability and higher residual activity than that of the free counterpart. Temperature investigations revealed that although the immobilized and free TLL presented the same temperature optima, the immobilized nanobiocatalyst exhibited enhanced heat resistance to a wider temperature range, retaining more than 53.3% of the maximum activity among the tested temperatures, as presented in Figure 5B. These positive changes might be associated with the charge of the various functional groups including amino groups in immobilization carriers [25], which interact with enzyme protein by covalent bond formation and ensure the conformational integrity and adjustability, thus reducing the sensitivity of pH and temperature. Previous studies reported a similar phenomenon of the behavior of the immobilized enzyme on nanomaterials [14,26].

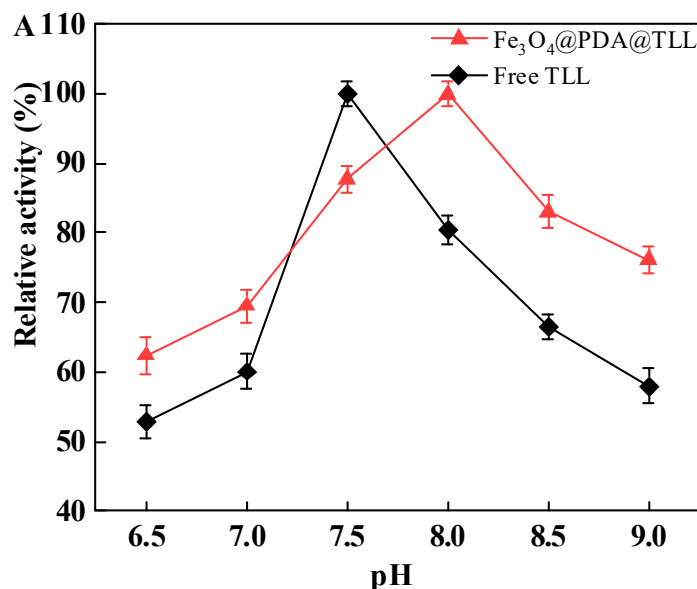
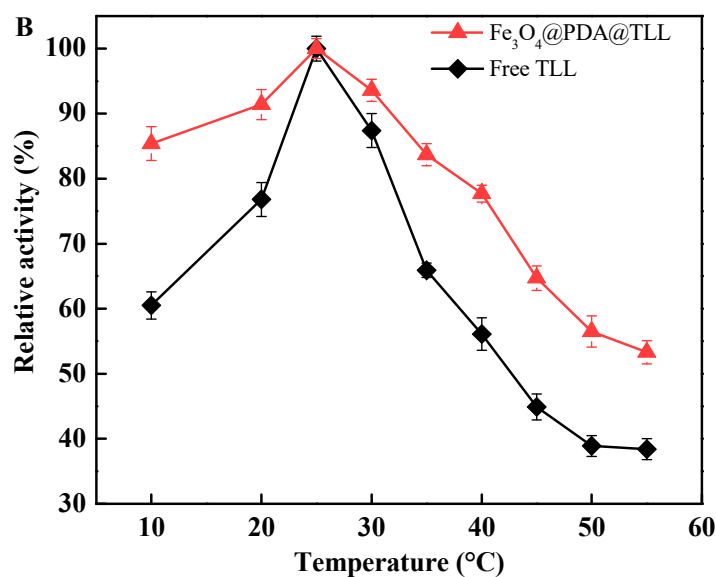


Figure 5. Cont.



**Figure 5.** Effect of pH (A) and temperature (B) on the activity of free TLL and Fe<sub>3</sub>O<sub>4</sub>@PDA@TLL.

#### 3.4. Stability of Free and Immobilized TLL

In addition to facilitating recovery for reuse, the increase in volume-specific enzyme loading, and simplification of downstream processing, another significant driving force for exploring novel immobilization techniques to immobilize biocatalyst is to achieve higher stability towards environmental perturbations. This is of both commercial and scientific interest [4,13]. The pH stability profile illustrates that the residual catalytic activity of Fe<sub>3</sub>O<sub>4</sub>@PDA@TLL was apparently higher than the free form after incubation for 12 h at the corresponding pH from 6.0–10, especially at the optimal pH of 8.0, with a 20.3% improvement of the relative activity, see Figure 6A. This confirms previous findings of pH effect on the behavior of the immobilized enzyme. Of the examined temperatures ranging from 25 °C to 80 °C depicted in Figure 6B, although the residual activities of Fe<sub>3</sub>O<sub>4</sub>@PDA@TLL and free TLL exhibited decreasing tendency, their retained activities in the whole temperature range are rather different. For free TLL, the relative activity drastically reduces from 100% to 17.5%, indicating poor stability to temperature. On the other hand, the immobilized Fe<sub>3</sub>O<sub>4</sub>@PDA@TLL exerted a considerably enhanced stability in the same temperature range, and retained 35.1% activity even at 80 °C. The reason for these phenomena might be that the immobilization effectively protects the protein subunit from unfolding and limits the conformation transition of the enzyme protein, thus strengthening the rigidity of the spatial conformation of the enzyme protein and leading to improvement of the heat stability [27].

Satisfactory solvent tolerance of the biocatalysts has been proven to be an essential characteristic and provides the non-aqueous enzymatic catalysis industry with a potentially wide application [4,28]. As is evident from the results in Figure 6C that Fe<sub>3</sub>O<sub>4</sub>@PDA@TLL displayed substantially higher catalytic activity as compared to the free enzyme in all the examined solvents. For instance, after a 12 h-incubation period in the strong-polar organic DMSO which can easily result in enzyme inactivation by stripping the essential water layer off the enzyme molecules [29], the immobilized TLL still achieved 2.0 times higher activity recovery (61.3% versus 30.1%) compared to that of the free enzyme. In contrast to traditional solvents, the four eco-friendly ChCl-based DESs, which have proved to be a sustainable and promising alternative to conventional organic media [30], showed good to excellent capacity to maintain enzyme activity, especially for the immobilized Fe<sub>3</sub>O<sub>4</sub>@PDA@TLL. In ChCl/GL (1:2), for example, the recovered activity of the immobilized TLL was 88.5%, which is higher than that of the free enzyme. Nearly all of the activity of the free TLL was lost after incubation in ChCl/AA, while the immobilized biocatalyst still exhibited a notable activity (34.4% of initial activity). Moreover, as evident from the data depicted in Figure 6D, the immobilized lipase still retained more than 70.2% of its original

activity even after being repeatedly employed for eight batches, suggesting that  $\text{Fe}_3\text{O}_4@\text{PDA@TLL}$  had satisfactory operational stability in the examined system.

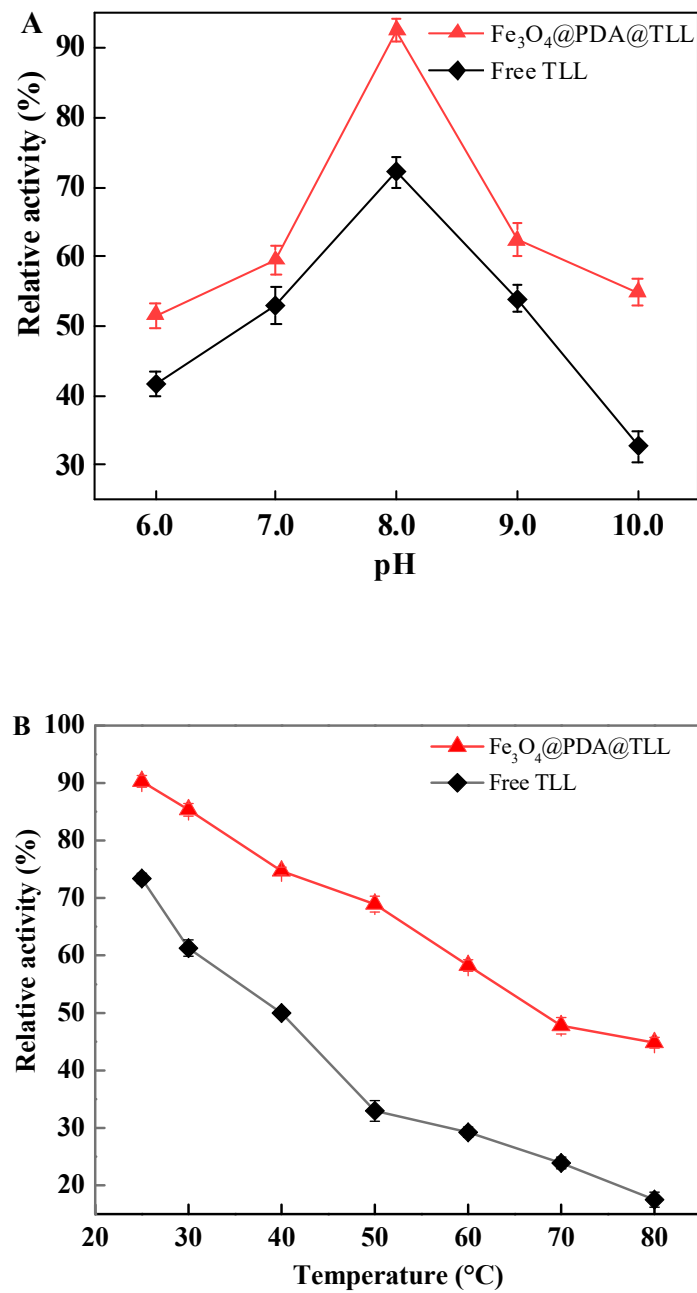


Figure 6. Cont.

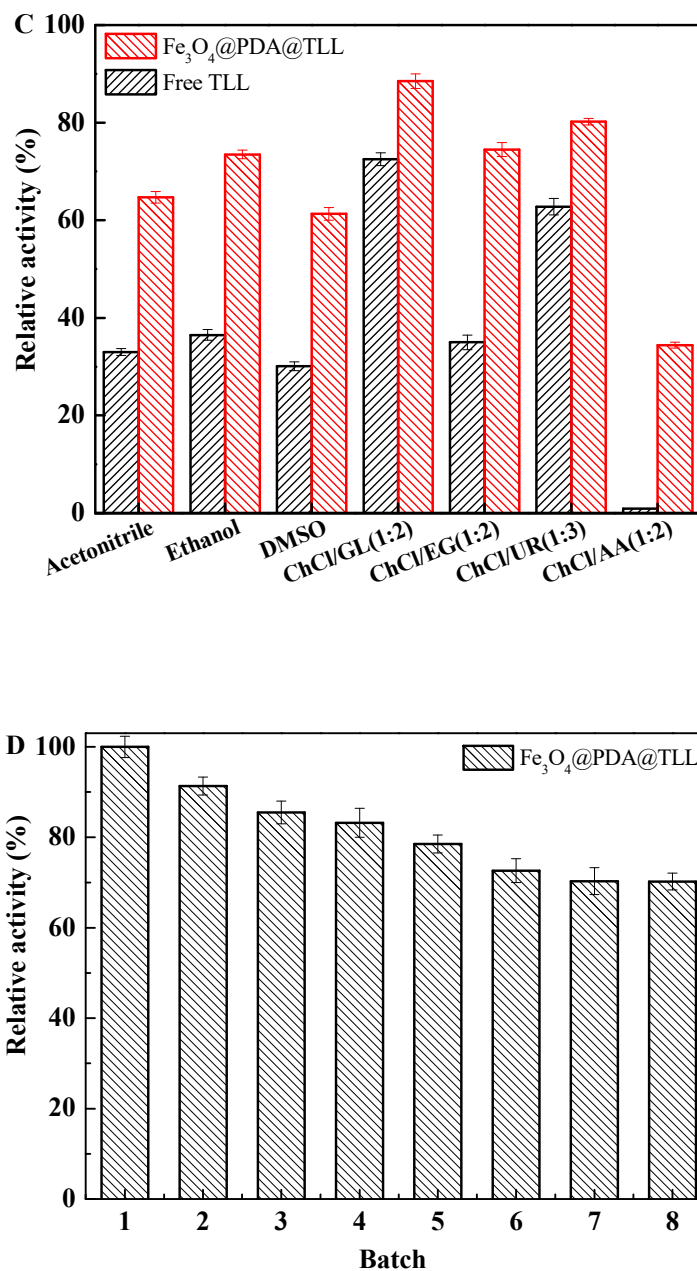


Figure 6. pH (A), thermal (B), solvent tolerance (C), and operational (D) stabilities of the enzyme.

#### 4. Conclusions

In conclusion, *T. lanuginosus* lipase was successfully immobilized on Fe<sub>3</sub>O<sub>4</sub>@PDA, which was prepared as a biocompatible matrix and characterized by TEM, FT-IR, XRD, WPS, and DLS with regard to their morphology, composition, and structure characteristics. The hydrolysis of *p*-NPP in phosphate buffer served as a model reaction to examine the catalytic properties of the immobilized enzyme. The results reported in this paper clearly show that Fe<sub>3</sub>O<sub>4</sub>@PDA@TLL exhibited much better resistance against pH, thermal, and solvent denaturation and satisfactory recyclability for *p*-NPP hydrolysis. Taken together, these findings demonstrated a promising application potential of the composite particles for enzyme immobilization.

**Author Contributions:** Conceptualization, Z.W., Z.J.; Investigation, Y.B., R.Z.; Methodology, Y.B., Z.W.; Project administration, Z.W.; Supervision, Z.J.; Writing—original draft, Y.B., Y.D.; Writing—review and editing, Y.T. All authors have read and agreed to the published version of the manuscript.

**Funding:** This research received no external funding.

**Acknowledgments:** This research was sponsored by the National Natural Science Foundation of China (Nos. 21676114 and 21706088), Qing Lan Project of Jiangsu Province of China, Six Talent Peaks Project in Jiangsu Province (No. SWYY-011; YY-061), and Graduate Research and Innovation Projects of Jiangsu Province (No. SJCX20\_0898) for financial support.

**Conflicts of Interest:** The authors declare no conflict of interest.

## References

1. Sheldon, R.A.; Van Pelt, S. Enzyme immobilisation in biocatalysis: Why, what and how. *Chem. Soc. Rev.* **2013**, *42*, 6223–6235. [CrossRef] [PubMed]
2. Guisan, J.M.; Bolivar, J.M.; López-Gallego, F.; Rocha-Martín, J. *Immobilization of Enzymes and Cells: Methods and Protocols*; Methods in Molecular Biology; Humana: New York, NY, USA, 2020. Available online: <https://link.springer.com/book/10.1007%2F978-1-0716-0215-7> (accessed on 5 May 2020).
3. Liang, S.; Wu, X.L.; Xiong, J.; Zong, M.H.; Lou, W.Y. Metal-organic frameworks as novel matrices for efficient enzyme immobilization: An update review. *Coordin. Chem. Rev.* **2020**, *406*, 213149. [CrossRef]
4. Adlercreutz, P. Immobilisation and application of lipases in organic media. *Chem. Soc. Rev.* **2013**, *42*, 6406–6436. [CrossRef] [PubMed]
5. Cao, S.L.; Xu, P.; Ma, Y.Z.; Yao, X.X.; Yao, Y.; Zong, M.H.; Li, X.H.; Lou, W.Y. Recent advances in immobilized enzymes on nanocarriers. *Chinese J. Catal.* **2016**, *37*, 1814–1823. [CrossRef]
6. Bilal, M.; Zhao, Y.P.; Rasheed, T.; Iqbal, H.M. Magnetic nanoparticles as versatile carriers for enzymes immobilization: A review. *Int. J. Biol. Macromol.* **2018**, *120*, 2530–2544. [CrossRef]
7. Xiao, D.L.; Lu, T.; Zeng, R.; Bi, Y.P. Preparation and highlighted applications of magnetic microparticles and nanoparticles: A review on recent advances. *Microchim. Acta* **2016**, *183*, 2655–2675. [CrossRef]
8. Oroujeni, M.; Kaboudin, B.; Xia, W.; Jönsson, P.; Ossipov, D.A. Conjugation of cyclodextrin to magnetic Fe<sub>3</sub>O<sub>4</sub> nanoparticles via polydopamine coating for drug delivery. *Prog. Org. Coat.* **2018**, *114*, 154–161. [CrossRef]
9. Cipolatti, E.P.; Valerio, A.; Henriques, R.O.; Moritz, D.E.; Ninow, J.L.; Freire, D.M.; Manoel, E.A.; Fernandez-Lafuente, R.; de Oliveira, D. Nanomaterials for biocatalyst immobilization—state of the art and future trends. *RSC Adv.* **2016**, *6*, 104675–104692. [CrossRef]
10. Cao, S.L.; Xu, H.; Lai, L.H.; Gu, W.M.; Xu, P.; Xiong, J.; Yin, H.; Li, X.H.; Ma, Y.Z.; Zhou, J. Magnetic ZIF-8/cellulose/Fe<sub>3</sub>O<sub>4</sub> nanocomposite: Preparation, characterization, and enzyme immobilization. *Bioresour. Bioprocess.* **2017**, *4*, 1–7. [CrossRef]
11. Wang, J.F.; Liu, Z.M.; Zhou, Z.M. Improving pullulanase catalysis via reversible immobilization on modified Fe<sub>3</sub>O<sub>4</sub>@ polydopamine nanoparticles. *Appl. Biochem. Biotech.* **2017**, *182*, 1467–1477. [CrossRef]
12. Fernandez-Lafuente, R. Lipase from *Thermomyces lanuginosus*: Uses and prospects as an industrial biocatalyst. *J. Mol. Catal. B-Enzym.* **2010**, *62*, 197–212. [CrossRef]
13. Gonçalves Filho, D.; Silva, A.G.; Guidini, C.Z. Lipases: Sources, immobilization methods, and industrial applications. *Appl. Microbiol. Biot.* **2019**, *103*, 7399–7423. [CrossRef] [PubMed]
14. Matuog, N.; Li, K.; Yan, Y.J. *Thermomyces lanuginosus* lipase immobilized on magnetic nanoparticles and its application in the hydrolysis of fish oil. *J. Food Biochem.* **2018**, *42*, e12549. [CrossRef]
15. Sarno, M.; Iuliano, M.; Polichetti, M.; Ciambelli, P. High activity and selectivity immobilized lipase on Fe<sub>3</sub>O<sub>4</sub> nanoparticles for banana flavour synthesis. *Process Biochem.* **2017**, *56*, 98–108. [CrossRef]
16. Ghasemi, S.; Sadighi, A.; Heidary, M.; Bozorgi-Koushalshahi, M.; Habibi, Z.; Faramarzi, M.A. Immobilisation of lipase on the surface of magnetic nanoparticles and non-porous glass beads for regioselective acetylation of prednisolone. *IET Nanobiotechnol.* **2013**, *7*, 100–108. [CrossRef]
17. Bradford, M.M. A rapid and sensitive method for the quantitation of microgram quantities of protein utilizing the principle of protein-dye binding. *Anal. Biochem.* **1976**, *72*, 248–254. [CrossRef]
18. Soni, S.; Dwivedee, B.P.; Banerjee, U.C. Facile fabrication of a recyclable nanobiocatalyst: Immobilization of *Burkholderia cepacia* lipase on carbon nanofibers for the kinetic resolution of a racemic atenolol intermediate. *RSC Adv.* **2018**, *8*, 27763–27774. [CrossRef]
19. Wang, C.H.; Han, H.B.; Jiang, W.; Ding, X.B.; Li, Q.S.; Wang, Y.B. Immobilization of thermostable lipase QLM on core-shell structured polydopamine-coated Fe<sub>3</sub>O<sub>4</sub> nanoparticles. *Catalysts* **2017**, *7*, 49. [CrossRef]

20. Cheng, G.; Zheng, S.Y. Construction of a high-performance magnetic enzyme nanosystem for rapid tryptic digestion. *Scientific Rep.* **2014**, *4*, 6947. [[CrossRef](#)]
21. Deng, X.; Cao, S.L.; Li, N.; Wu, H.; Smith, T.J.; Zong, M.H.; Lou, W.Y. A magnetic biocatalyst based on mussel-inspired polydopamine and its acylation of dihydromyricetin. *Chin. J. Catal.* **2016**, *37*, 584–595. [[CrossRef](#)]
22. Sureshkumar, M.; Lee, C.K. Polydopamine coated magnetic-chitin (MCT) particles as a new matrix for enzyme immobilization. *Carbohydr. Polym.* **2011**, *84*, 775–780. [[CrossRef](#)]
23. Wang, X.Y.; Jiang, X.P.; Li, Y.; Zeng, S.; Zhang, Y.W. Preparation Fe<sub>3</sub>O<sub>4</sub>@chitosan magnetic particles for covalent immobilization of lipase from *Thermomyces lanuginosus*. *Int. J. Biol. Macromol.* **2015**, *75*, 44–50. [[CrossRef](#)] [[PubMed](#)]
24. Xia, T.T.; Liu, C.Z.; Hu, J.H.; Guo, C. Improved performance of immobilized laccase on amine-functionalized magnetic Fe<sub>3</sub>O<sub>4</sub> nanoparticles modified with polyethylenimine. *Chem. Eng. J.* **2016**, *295*, 201–206. [[CrossRef](#)]
25. Kumar, D.; Nagar, S.; Bhushan, I.; Kumar, L.; Parshad, R.; Gupta, V.K. Covalent immobilization of organic solvent tolerant lipase on aluminum oxide pellets and its potential application in esterification reaction. *J. Mol. Catal. B-Enzym.* **2013**, *87*, 51–61. [[CrossRef](#)]
26. Wang, J.Z.; Zhao, G.H.; Jing, L.Y.; Peng, X.M.; Li, Y.F. Facile self-assembly of magnetite nanoparticles on three-dimensional graphene oxide–chitosan composite for lipase immobilization. *Biochem. Eng. J.* **2015**, *98*, 75–83. [[CrossRef](#)]
27. Marruecos, D.F.; Schwartz, D.K.; Kaar, J.L. Impact of surface interactions on protein conformation. *Curr. Opin. Colloid Interface Sci.* **2018**, *38*, 45–55. [[CrossRef](#)]
28. Salihu, A.; Alam, M.Z. Solvent tolerant lipases: A review. *Process Biochem.* **2015**, *50*, 86–96. [[CrossRef](#)]
29. Yang, R.L.; Zhao, X.J.; Wu, T.T.; Bilal, M.; Wang, Z.Y.; Luo, H.Z.; Yang, W.J. A novel and highly regioselective biocatalytic approach to acetylation of helicid by using whole-cell biocatalysts in organic solvents. *Catal. Commun.* **2019**, *128*, 105707. [[CrossRef](#)]
30. Pätzold, M.; Siebenhaller, S.; Kara, S.; Liese, A.; Syldatk, C.; Holtmann, D. Deep eutectic solvents as efficient solvents in biocatalysis. *Trends Biotechnol.* **2019**, *37*, 943–959. [[CrossRef](#)]



© 2020 by the authors. Licensee MDPI, Basel, Switzerland. This article is an open access article distributed under the terms and conditions of the Creative Commons Attribution (CC BY) license (<http://creativecommons.org/licenses/by/4.0/>).